

## THE STATIC AND DYNAMIC COMPRESSIVE BEHAVIOUR OF SELECTED ALUMINIUM ALLOYS

R. Winzer, A. Glinicka

**Warsaw University of Technology**  
**Faculty of Civil Engineering**  
**Department for Strength of Materials**  
16 Armii Ludowej Av., 00-637 Warsaw, Poland  
e-mail: {r.winzer, a.glinicka}@il.pw.edu.pl

The mechanical properties of structural aluminium alloys EN AW-5083 and EN AW-6082 in the ‘H111’ and ‘T6’ conditions, respectively, subjected to compressive loadings in the quasi-static and dynamic strain rate regimes, are investigated. Both alloys are used as structural components not only in car body design or ship building, but also in civil engineering. Therefore, compression tests at room temperature were conducted using a servohydraulic Instron machine, in order to determine the materials’ behaviour at low and intermediate rates of deformation. In addition, to predict the dynamic response of these materials, the Split Hopkinson Pressure Bar (SHPB) technique was utilized. For alloy 5083-H111, a changeover from negative to positive strain rate sensitivity at dynamic strain rates is observable, whilst alloy 6082-T6 exhibits a mild trend towards positive strain-rate sensitivity. Furthermore, the coefficients of the Johnson-Cook model, that are valid under dynamic conditions, are determined. The finite element simulation of SHPB experiments shows that the constitutive model represents the materials’ behaviour quite well.

### 1. INTRODUCTION

Aluminium alloys are a flexible and attractive material for use in many applications. The desire for optimal design of structures with high mechanical capacity and light-weight properties, does not only play a significant role in aerospace engineering. In view of shorter becoming supply of resources, the aspect of minimisation of weight is also crucial in car manufacturing and ship-building. Therefore, light-weight materials like aluminium alloys are already applied as structural materials during the design process. Moreover, automotive crashworthiness plays an important role in the design of passenger cars. In order to manage the energy of a collision in a reliable manner in the event of a car accident or ship collision, the energy absorption performance needs to be understood. Thus, the stress-strain relationship for dynamic strain rates should be studied.

Due to its high ratio of load-bearing capacity to weight combined with high corrosion resistance, what leads to lower maintenance requirements, aluminium alloys are also used in civil engineering. In addition, thanks to its recycling potential, it is a sustainable solution as a building material. Indeed, a classical field of aluminium's utilisation in civil engineering is its application as facade elements [1], but load-bearing aluminium structures can also be found [2], for example in bridge constructions. It can be determined that aluminium structures in civil engineering are subjected to loadings caused by wind, earthquake and impact, for instance. These loadings generate strain rates from  $10^{-4}$  up to  $10^4 \text{ s}^{-1}$ . Therefore, the material properties of two commercial aluminium alloys EN AW-5083 and EN AW-6082 in the 'H111' and 'T6' condition, respectively, at low and high rates of deformation are investigated. As mentioned in [3], the series 5xxx and 6xxx are most used for structural components in bridge building. Eurocode 9 [4] states that the first alloy is the strongest structural non-heat treatable alloy in general commercial use, possessing very good corrosion resistance in the marine environment. Therefore, it is utilised for structural parts of naval and offshore structures. On the other hand, the second alloy is one of the most widely used heat treatable high strength alloy with good corrosion resistance and good weldability.

Alloy composition, strain rate and temperature may have an effect on mechanical properties of aluminium alloys [5]. WAGENHOFER *et al.* [6] reported a reversed strain effect occurring at room temperature in alloy 5086. A negative strain rate sensitivity changed into a positive one at a strain rate nearly equal to  $1 \text{ s}^{-1}$ . Similarly, CLAUSEN *et al.* [7] revealed that alloy 5083 in 'H116' condition exhibits a negative strain rate sensitivity for strain rates up to  $1 \text{ s}^{-1}$ , but positive strain rate sensitivity in the dynamic strain rate regime. A changeover from negative to mild positive strain rate was also observed by HADIANFARD *et al.* [8] for 5xxx aluminium alloys. Aforementioned investigations considered the alloys' behaviour in tension. On the contrary, CHEN *et al.* [9] carried out experimental tests over a wide range of strain rates on 6xxx aluminium alloys in tension, namely on alloys 6060 and 6082 in tempers T6. The tests showed that both alloys exhibit only slight strain rate sensitivity, even a slight negative tendency for high strain rates is observable for both alloys, whilst LEE and KIM [10] disclosed that the flow stress of alloy 6061 in temper T6 exhibits an increase of 320 and 90% at compression and tension, respectively, for high rates of deformation. A distinctive sensitivity to the strain rate is visible. Thus, the objective of underlying work is to investigate the effects of strain rate on the mechanical properties of selected 5xxx and 6xxx aluminium alloys in compression. Hence, compression tests at room temperature were conducted using a servo-hydraulic Instron machine in order to determine the materials' behaviour at low and intermediate rates of deformation. In addition, to predict the response

caused by impact loading, the Split Hopkinson Pressure Bar (SHPB) technique was utilised. Moreover, for further FE analysis in future, constitutive material parameters were determined and validated.

## 2. EXPERIMENTAL PROCEDURE

### 2.1. The investigated materials

As mentioned above, the aluminium alloys EN AW-5083 and EN AW-6082 in tempers H111 and T6, respectively, were considered in this evaluation. Their main alloying elements are magnesium, manganese and silicon, magnesium. The chemical compositions of the materials are presented in Table 1. The alloys were provided as round bars with 16 or 10 mm diameters.

**Table 1. Chemical compositions of the alloys in wt.%.**

Alloy	Si	Fe	Cu	Mn	Mg	Cr	Zn	Ti
EN AW-5083	0.40	0.40	0.10	0.70	4.45	0.25	0.25	0.15
EN AW-6082	0.88	0.29	0.08	0.46	0.73	0.03	0.04	0.02

### 2.2. Static and quasi-static compression tests

Compression tests were carried out using a servohydraulic Instron machine (type 8802) at strain rates of  $10^{-4}$ ,  $10^{-3}$ ,  $10^{-2}$ ,  $10^{-1}$  and  $1 \text{ s}^{-1}$ , at room temperature. All tests were performed in displacement control with clamp velocity adapted to the corresponding strain rate. In order to specify a flow curve for cylindrical shaped metallic specimens, the initial ratio between length and diameter should be between 1 and 2. The samples' ratio was equal to 1.5 with an initial diameter of 10 mm in all cases. Three compression tests were at least conducted for each strain rate and alloy.

### 2.3. Dynamic compression tests

A variety of experimental techniques, such as Taylor impact or shock loading by plate impact, can be utilised to obtain high rates of strain. An interesting and detailed overview of these techniques can be found in [11]. A technique which enables to measure the response of materials at strain rates between  $10^2$ – $10^4 \text{ s}^{-1}$ , first introduced by KOLSKY [12], is the Split Hopkinson Pressure Bar (SHPB) apparatus. In general, this apparatus consists of an air gun, a striker bar, two Hopkinson bars (known as incident and transmitter bars), a velocity measuring device and recording equipment. The specimen is sandwiched between the two

bars. The dynamic compression tests were performed in the laboratory of the Division of Experimental Mechanics at the Institute of Fundamental Technological Research.

A schematic view of the SHPB apparatus is illustrated in Fig. 1. Both the incident and transmitter bars are made of spring steel, whose yield strength and elastic modulus are equal to 1180 MPa and 210 GPa, respectively. Their diameter and length are 20 and 1050 mm, respectively. The striker bar or projectile has the identical diameter and is made of the same steel. Three striker bars of varying length were used.

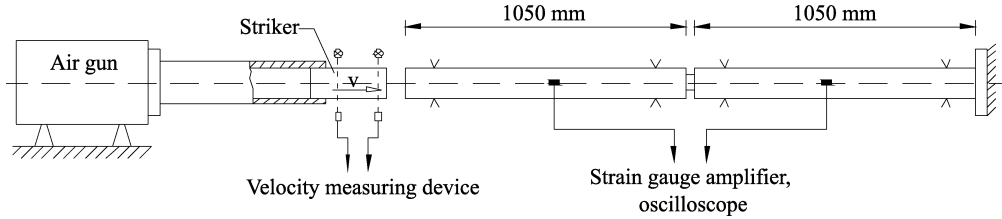


FIG. 1. Schematic view of SHPB apparatus.

First of all, the striker bar is fired by the air gun and impacts the incident bar. By reason of the impact, a nearly rectangular compressive stress and a strain pulse with very short rise time is generated, which propagates with the speed of sound  $c_0 = (E/\rho)^{1/2}$  along the incident bar until it hits the specimen, where  $E$  is the elastic modulus and  $\rho$  the bar's density. Propagating into the specimen, a part is transmitted into the transmitter bar, whilst the other part is reflected back into the incident bar as a tensile wave. During the test, the bars remain within their elastic limit. The incident, transmitted and reflected pulses  $\varepsilon_I$ ,  $\varepsilon_T$ , and  $\varepsilon_R$ , respectively, were measured using strain gauges (HBM LY11-1.5/120) attached to each bar. The strain gauges were connected with a strain gauge amplifier. Finally, the output signals of the strain gauges were visualized and stored in an oscilloscope (Agilent 54624A) at a sampling rate of 0.25  $\mu\text{s}$ . Figure 2 shows typical incident, transmitted and reflected voltage signals that were saved into the oscilloscope. The time-dependent strain rate can be determined by means of recorded strains as follows:

$$(2.1) \quad \dot{\varepsilon}_s = -\frac{2c_0}{l_0}\varepsilon_R,$$

where  $l_0$  is the initial length of the specimen. Thus, the strain as a function of time can be calculated by integrating the above equation from 0 to  $t$ ,

$$(2.2) \quad \varepsilon_s = -\frac{2c_0}{l_0} \int_0^t \varepsilon_R d\tilde{t}.$$

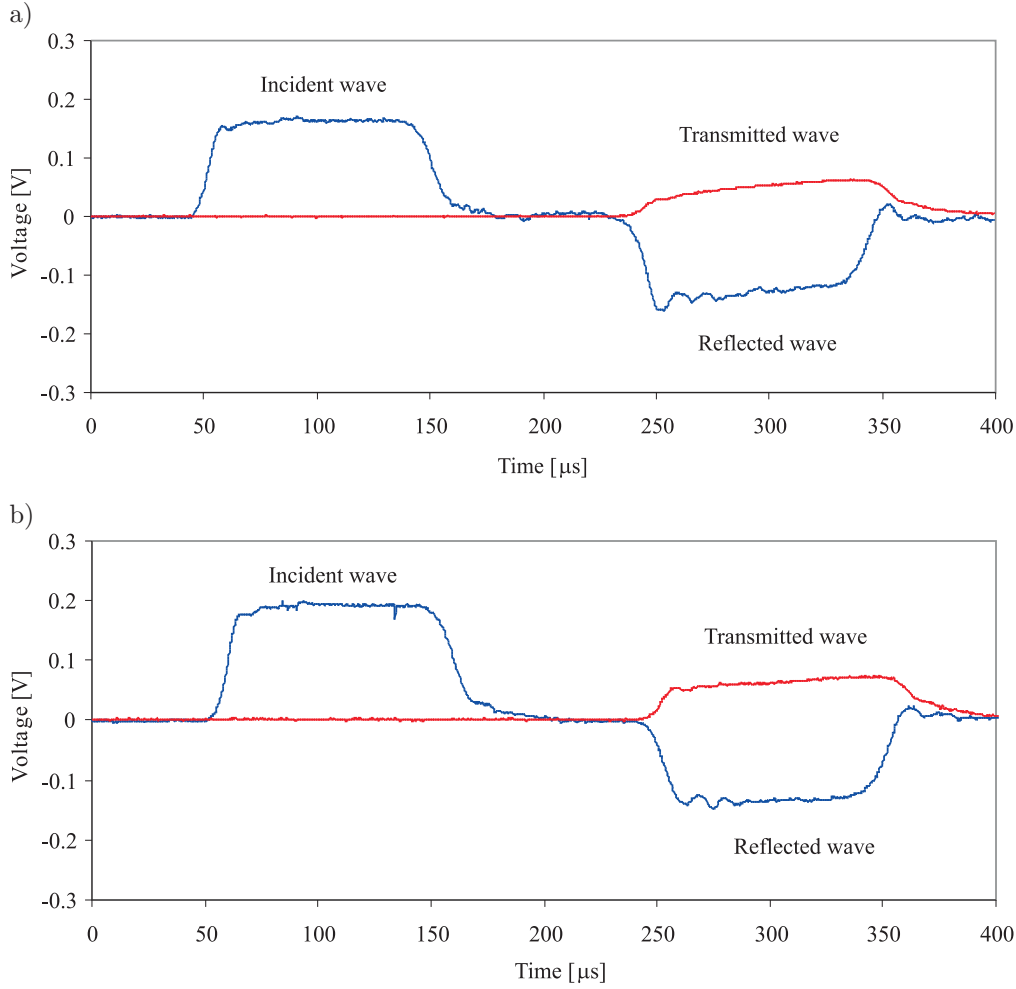


FIG. 2. Typical pulses for (a) 5083-H111 and (b) 6082-T6 aluminium alloy.

Considering force equilibrium at the contact faces of the bars, an average value for the stress on the specimen can be derived

$$(2.3) \quad \sigma_s = E \frac{A_b}{A_s} \varepsilon_T,$$

where  $A_b$  is the cross-sectional area of the incident bar and  $A_s$  is the cross-sectional area of the specimen.

A detailed derivation of Eqs. (2.1)–(2.3) can be found elsewhere [13, 14]. From the theoretical point of view, they are based on the one-dimensional propagation of elastic waves in a continuum including some basic assumptions. Namely, there exists force equilibrium on the interfaces during the process of deformation, i.e.

a uniform axial stress distribution is assumed, and both the friction and inertia forces are negligible. In order to reduce frictional effects, the interfaces between the specimen and the bars were lubricated. As recommended in [14, 15], to minimise the errors due to longitudinal and radial inertia forces, all specimens had an initial diameter and length of 10 and 5 mm, respectively. A special instrumentation was used to apply the specimen in the center of the bars. A further assumption is that the elastic wave travels along the bars without any damping. This is justified only if the ratio between wavelength and bar diameter is great enough, otherwise dispersion is clearly visible as shown by GORHAM and WU [16].

### 3. RESULTS OF STATIC AND DYNAMIC COMPRESSION TESTS

Henceforth, the nominal (engineering) strain and stress are used to calculate the true strain  $\varepsilon = \ln(1 + \varepsilon_{\text{nom}})$  and the true stress  $\sigma = \sigma_{\text{nom}}(1 + \varepsilon_{\text{nom}})$ . Figure 3 illustrates representative flow curves obtained during low and intermediate strain rate compression tests at room temperature. A considerable different trend is observed. For alloy 5083-H111, a negative strain rate effect is clearly visible, i.e. with increasing strain rate, a decreasing flow stress level is observable. For instance, at a plastic strain of 0.3 the flow stress decreased approximately by 15%. In contrast, a slight trend towards positive strain rate sensitivity for alloy 6082-T6 is shown, but this effect is not so distinctive as in the case of the previous alloy. Only an increase of nearly 3.5% could be found.

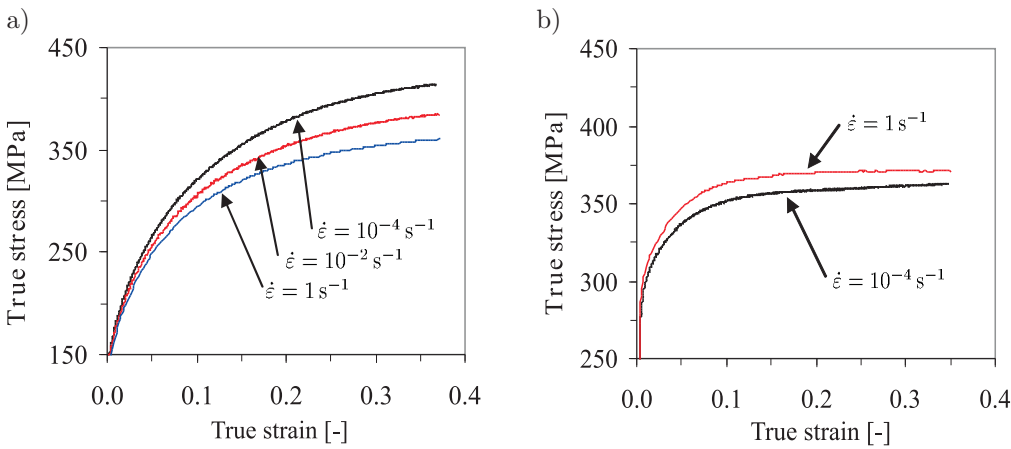


FIG. 3. Static flow curves of (a) 5083-H111 and (b) 6082-T6 aluminium alloy.

Furthermore, several tests have been conducted for each alloy by means of the SHPB apparatus. In Fig. 4, the obtained dynamic flow curves are illustrated.

For the sake of clarity, only hardening curves corresponding to low, intermediate and high impact velocities are shown. The maximum strain did not exceed the value of 0.4, whereas strain rates from 500 up to 5500  $\text{s}^{-1}$  have been achieved. Figure 4a clearly reveals that the flow stress level of aluminium alloy 5083-H111 increases with increasing strain rate. A change in the strain rate sensitivity can be recognized. The flow stress level of alloy 6082-T6 also increases with increasing strain rate, but very slightly. For a more precise analysis, the flow stress level at 0.05 true plastic strain is plotted as a function of strain rate in Fig. 5. A reduction of flow stress for alloy 5083-H111 can be clearly observed

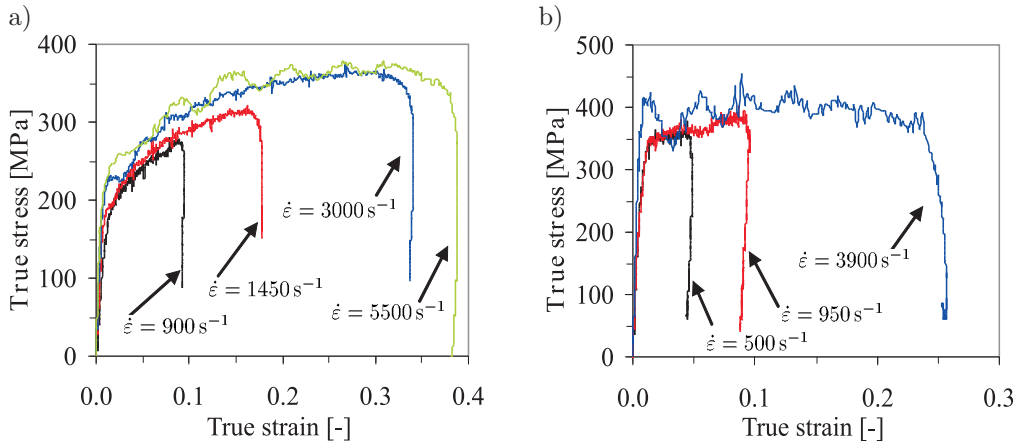


FIG. 4. Dynamic flow curves of (a) 5083-H111 and (b) 6082-T6 aluminium alloy.

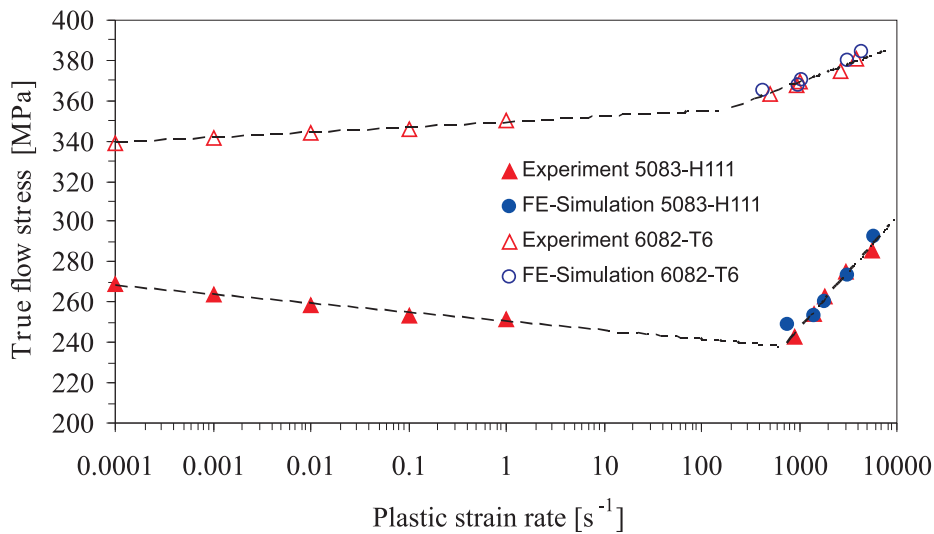


FIG. 5. True flow stress at 0.05 true plastic strain as a function of strain rate; comparison of numerical results.

for strain rates between  $10^{-4}$  and  $1 \text{ s}^{-1}$ . A decrease of approximately 10% could be found out. However, under dynamic conditions, the flow stress increases by about 25%. In contrast, aluminium alloy 6082-T6 is almost rate-insensitive, a decrease of nearly 3% at quasi-static strain rates is observed. A mild trend towards positive strain rate sensitivity can be noticed. The flow stress increased by about 8% under dynamic conditions.

Furthermore, the diameter of each specimen was measured prior and after the experiment in two or three radial directions. It was found out that the surface had a circular shape, i.e. not elliptical. This indicates that the alloys behave as isotropic. Therefore, the use of an isotropic yield criterion for numerical purposes is justified. Typical specimens are shown in Fig. 6. For samples B and C, strain rates of 950 and  $3000 \text{ s}^{-1}$  were calculated, their corresponding dynamic hardening curves are plotted in Fig. 4. Their initial and final lengths were 4.94, 4.98 and 3.48, 4.58 mm, respectively, what leads to a maximum strains of 0.35 and 0.08, respectively.

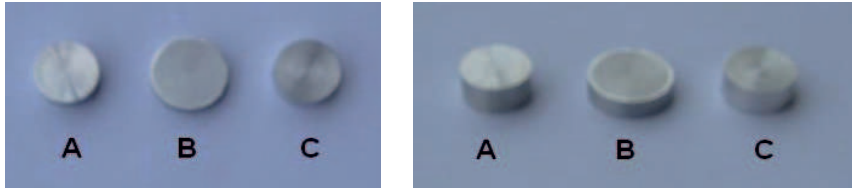


FIG. 6. Examples of typical specimens used for dynamic investigations, prior to experiment (A), and aluminium alloy 5083-H111 (B) and 6082-T6 (C) samples after compression.

#### 4. NUMERICAL SIMULATIONS

In order to verify the constitutive model, a finite element simulation of the Hopkinson bar test was performed. Since stress wave propagation is a typical application for an explicit finite element code, the commercial software ABAQUS/Explicit, well-suited for high-speed dynamic events [17], was used.

##### 4.1. Basic formulations, constitutive equation and parameter identification

When the elastic strains are small (negligible compared to unity) in a large deformation analysis, the additive decomposition of the rate-of-deformation tensor into elastic and plastic parts is assumed (see, e.g. BELYTSCHKO *et al.* [18])

$$(4.1) \quad \mathbf{D} = \mathbf{D}^e + \mathbf{D}^p,$$

where  $\mathbf{D}$  is defined as the symmetric part of the velocity gradient as follows:

$$(4.2) \quad \mathbf{D} = \text{sym } \mathbf{L} = \text{sym} \frac{\partial v}{\partial x}.$$

Henceforth, a hypoelastic-viscoplastic isotropic material is considered. Then, ABAQUS computes the plastic part of the rate-of-deformation tensor by means of the associated flow rule:

$$(4.3) \quad \mathbf{D}^p = \lambda \frac{\partial f}{\partial \boldsymbol{\sigma}} = \frac{3 \bar{\varepsilon}^p}{2 \bar{\sigma}} \mathbf{s}.$$

In this equation  $\mathbf{s}$  is the deviatoric part of the stress tensor, whilst  $\bar{\varepsilon}^p$  is the equivalent plastic strain. To characterise the yield behaviour of metals, what means incompressible behaviour beyond the elastic limit, a yield function of von Mises type is considered

$$(4.4) \quad f = \sqrt{\frac{3}{2}} \|\mathbf{s}\| - \bar{\sigma}.$$

To ensure objectivity, the finite element programme uses a linear hypoelastic relation based on the Green-Naghdi stress rate tensor

$$(4.5) \quad \boldsymbol{\sigma}^{\nabla G} = \dot{\boldsymbol{\sigma}} - \boldsymbol{\Omega} \cdot \boldsymbol{\sigma} + \boldsymbol{\sigma} \cdot \boldsymbol{\Omega} = \mathbb{C} : \mathbf{D}^e,$$

where  $\boldsymbol{\Omega}$  and  $\mathbb{C}$  are the angular velocity tensor and the fourth-order elastic stiffness tensor, respectively. Moreover, the plastic behaviour of the specimen as a function of strain, strain rate and temperature can be specified by the Johnson-Cook constitutive equation [19]. In particular, this constitutive relation reads

$$(4.6) \quad \bar{\sigma} = (A + B(\bar{\varepsilon}^p)^n) \left( 1 + C \ln \left( \frac{\dot{\bar{\varepsilon}}^p}{\dot{\varepsilon}_0} \right) \right) (1 - \hat{T}^m).$$

The term in the last parenthesis accounts for thermal softening of the material. In the case of  $T_r$  and  $T_m$  being the room and melting temperature, respectively, then  $\hat{T}$  is defined as

$$(4.7) \quad \hat{T} = \frac{T - T_r}{T_m - T_r}.$$

As mentioned in [9], investigations by CLAUSEN *et al.* [7] and BØRVIK *et al.* [20] revealed that a temperature rise up to 100°C does not affect the mechanical behaviour in a critical manner. An estimation of the temperature rise in this work is found to be 38°C. Due to the latter and the fact that all tests were carried out at room temperature,  $\hat{T}$  was set a priori equal to zero. In order to determine the other coefficients, a reference stress-strain curve with a reference strain rate needs to be chosen. Thus, the parameter  $\dot{\varepsilon}_0$  is determined. The reference strain rate for alloys 5083-H111 and 6082-T6 were chosen to be 1450 and 1000 s<sup>-1</sup>, respectively. Afterwards, the coefficients in the first parenthesis can be determined, whereas the value of  $A$  can be identified as the yield stress.

In the next step,  $B$  and  $n$  can be calculated by means of the least square method. Aforementioned procedure was repeated for each test, so all stress-strain curves have analytical forms. Finally, the parameter  $C$  can be specified by rearranging Eq. (4.6) with respect to parameter  $C$ . The parameters for the alloys are listed in Table 2, but one should note the following: namely, since  $C$  must have a positive value due to the fact that selected model requires a positive strain rate the use of the model is only justified for situations where dynamic strain rates emerge. So, negative strain rate sensitivity of alloy 5083-H111 in the static and quasi-static dynamic strain rate regime cannot be modelled via the determined coefficients. Moreover, it is possible to ascertain additional Johnson-Cook parameters for alloy 6082-T6 that are valid for low and intermediate rates of deformation, but within this strain rate regime the alloy can also be modelled as rate-insensitive. The experimental results show that this alloy exhibits only a slight sensitivity to the strain rate (cf. Fig. 4b); therefore, the coefficient has only a slight value.

**Table 2. Parameters in the Johnson-Cook constitutive equation.**

Alloy	$A$ [MPa]	$B$ [MPa]	$n$ [-]	$C$ [-]
EN AW- 5083	147.0	349.2	0.396	0.104
EN AW- 6082	307.8	145.7	0.288	0.02519

#### 4.2. Finite element model and numerical results

In general, the model consists of two elastic bars with a Young's modulus of 210 GPa and Poisson's ratio equal to 0.3, and a specimen which is sandwiched between these two bars. A third bar (striker bar) hits the free end of the incident bar. This experimental setup was modelled taking the double symmetry into account (cf. Fig. 7). Eight-node hexahedron elements with reduced integration were used to model all parts. A surface to surface contact was considered between the respective interfaces.

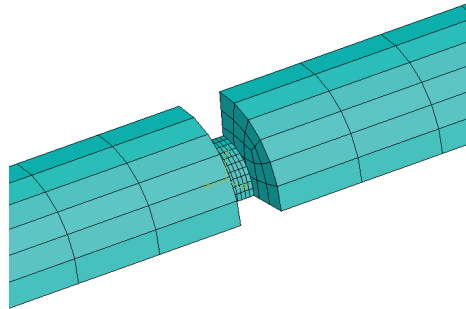


FIG. 7. Finite element mesh of SHPB setup.

The initial compressive stress wave can be simulated via the impact of the striker bar at the free end of the incident bar. Another possibility is to subject the free end of the bar to a blast load. Both possibilities have been performed leading to the same results. Moreover, the analytical solution of one-dimensional wave equation assumes that the specimen is subjected to a Heaviside step load of an infinite duration. Indeed, this zero rise time assumption is not realistic. In practice, however, the pulse shape is trapezoidal and is distorted as a result of wave dispersion. As shown in Fig. 8b, in the time domain, dispersion is observable as oscillations. Thus, using finite element simulation, the pulse shape caused by the impact or rather the blast load should be trapezoidal. RAMÍREZ and RUBIO-GONZALEZ [21] demonstrated that the higher, is the rise time, the lower will be the dispersion effects. This is important, since wave dispersion is able to limit the accuracy of the obtained results, especially for lower impact velocities, where the rise time during the experiment takes a longer period. The pulse shape effect on wave dispersion is presented in Fig. 8, a longer rise time leads to reduced dispersion effects. A trapezoidal blast load fits better to experimental data and is, therefore, more realistic (cf. Fig. 8b). Earlier observations in [21] are in good agreement with experimental and numerical results of this work.

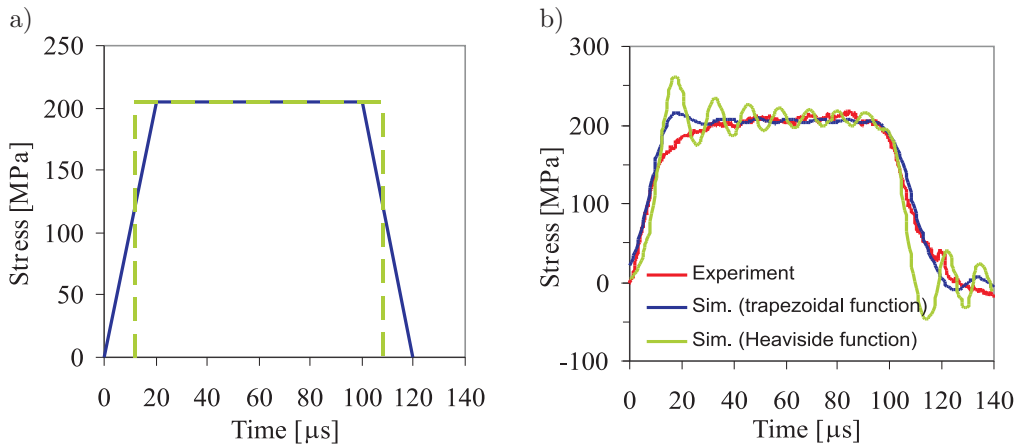
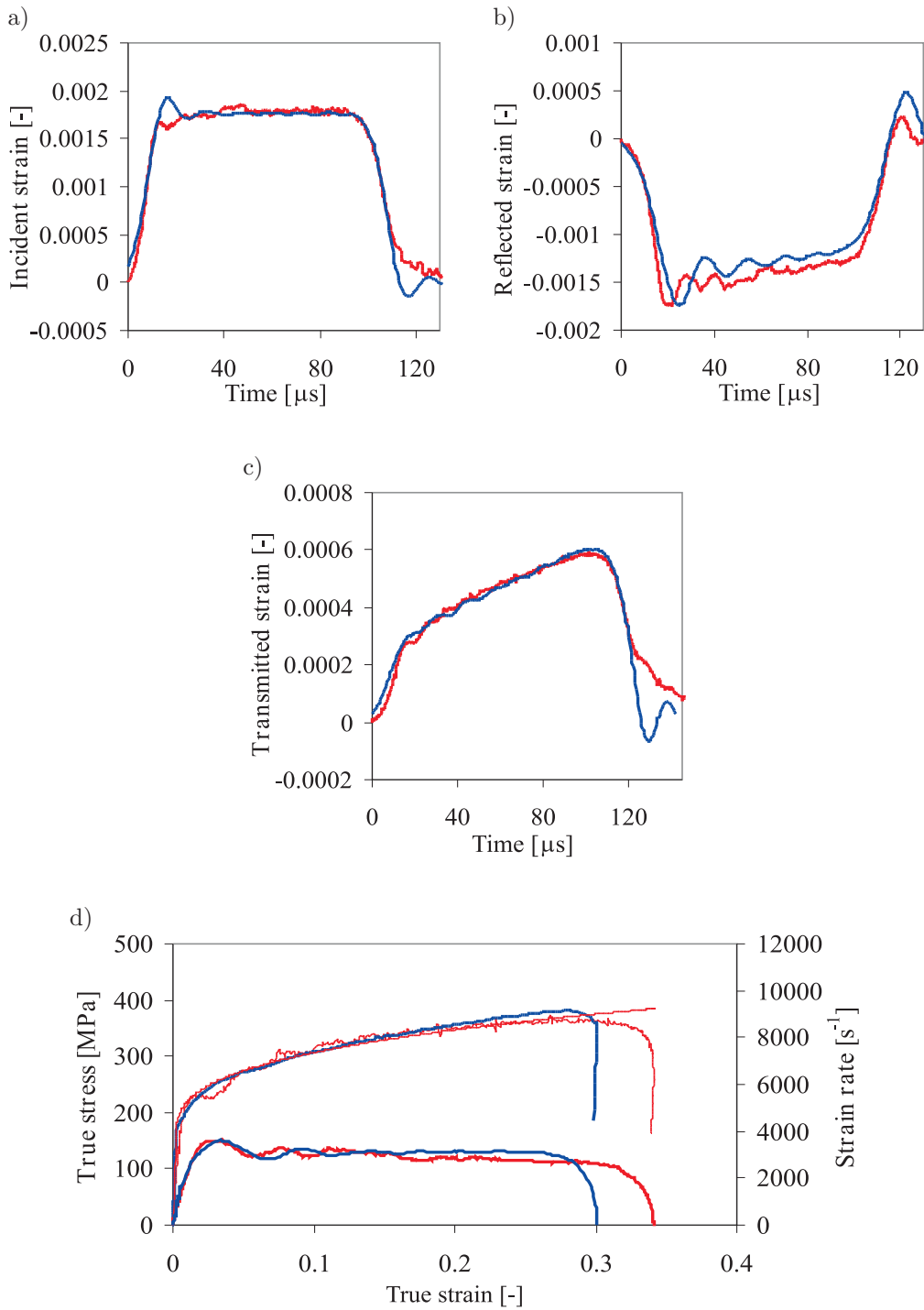


FIG. 8. (a) Trapezoidal and Heaviside step load, (b) comparison between experimental and simulated incident pulses.

All tests for each alloy have been simulated. In general, the numerical results represent the experimental findings with adequate accuracy. In Fig. 9 a comparison between numerical and experimental results for both alloys is presented, their stress-strain relations were already presented in Fig. 4. All strain pulses are simulated reasonably well, as shown in Fig. 9a-c. The aforementioned pulses are



[FIG. 9a-d]

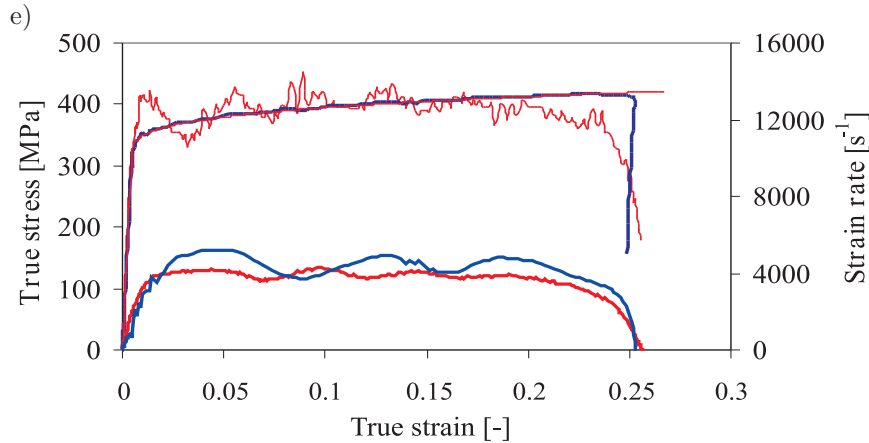


FIG. 9. Comparison between (red line) experimental and (blue line) numerical results; representative (a) incident, (b) reflected, (c) transmitted strain pulse, (d) stress-strain and strain rate-strain curve for alloy 5083-H111 and (e) stress-strain and strain rate-strain curve for alloy 6082-T6.

related to Fig. 9d, whilst in Fig. 9e only the dynamic hardening curve with the corresponding strain rate-strain relation for alloy 6082-T6 is presented. In case of alloy 5083-H111, the obtained maximum strains in the finite element simulations are slightly shorter compared to the experimental strains, whilst in case of the other alloy, both strains agree much better. Nevertheless, it can be observed that the Johnson-Cook model represents the flow stress level of both alloys quite well. All this can be confirmed when Fig. 5 is considered. The flow stress obtained by the experiments and simulations at 0.05 true plastic strain, can be compared with each other at a wide range of strain rates. A good agreement with the experimental data is observable.

## 5. CONCLUSIONS

Compression tests on two structural aluminium alloys over a wide range of strains and strain rates were performed. To obtain quasi-static strain rates, a servohydraulic Instron machine was utilised, whilst a Split Hopkinson Pressure Bar was applied in order to obtain high strain rates.

The experimental findings reveal that the alloy 5083 in temper H111 exhibits a negative strain rate sensitivity in the quasi-static strain rate regime, whilst a positive strain rate sensitivity is observable in the dynamic strain rate regime. Alloy 6082 in temper T6 is almost rate-insensitive for strain rates up to  $1 \text{ s}^{-1}$ . Above this strain rate, a slight positive strain rate sensitivity can be noticed. Unfortunately, an exact value of the turning point in case of alloy 5083-H111

could not be determined due to lack of experimental data in the range of 10–500 s<sup>-1</sup>. A logarithmic interpolation through the data points in Fig. 5 would lead to a value of approximately 600 s<sup>-1</sup>. To achieve this intermediate or “sub-Hopkinson” strain rates, a servohydraulic machine must be used which enables higher clamp velocities. However, as mentioned by other authors [6, 8], the two test devices, namely the servohydraulic machine in conjunction with the SHPB apparatus, can be applied in order to obtain consistent experimental data. Despite the lack of experimental data it is visible to the naked eye (cf. Fig. 5) that intermediate strain rate data points fit well with data points in the dynamic strain rate regime. No sudden change in the flow stress level indicating a source of error is visible.

Moreover, the parameters in the Johnson-Cook constitutive equation were calibrated (cf. Table 2). Since it is not possible to simulate negative strain rate sensitivity by means of this model, the calculated parameters are only valid under dynamic conditions, i.e. for strain rates above ca. 500 s<sup>-1</sup>. In case of alloy 6082-T6, the parameters are also valid under dynamic conditions, this means for strain rates exceeding the value of ca. 100 s<sup>-1</sup>. For strain rates below 100 s<sup>-1</sup> this alloy can be modelled as rate-insensitive. In order to validate the constitutive model, a finite element simulation of the Split Hopkinson Pressure Bar test was performed. Both the strain hardening and strain rate hardening could be represented via this model adequately. It can be determined that the numerical results fit very well to the experimental data.

#### ACKNOWLEDGEMENTS

Support for the present work was provided by the Warsaw University of Technology under rector’s grant no. 503G 1083 0100 009. Furthermore, the authors would like to thank Dr. Artur Zbiciak for numerous and fruitful discussions and Professor Zbigniew L. Kowalewski for giving them the opportunity to conduct their dynamic experiments in the laboratory of the Division of Experimental Mechanics, at the Institute of Fundamental Technological Research.

#### REFERENCES

1. H. WILQUIN, *Aluminium in Building – Construction and Design* [in German], Birkhäuser Verlag für Architekten, Berlin, 2001.
2. G. VALTINAT, *Aluminium in Structural Engineering* [in German], Ernst & Sohn, 2003.
3. T. SIWOWSKI, *Aluminium road bridges – past, present and future* [in Polish], *Drogi i Mosty*, **1**, 39–73, 2005.

4. Eurocode 9, ENV 1999-1-1, *Design of aluminium structures – Part 1.1: General rules – General rules and rules for buildings*, 1997.
5. A. M. BRAGOV and A. K. LUMANOV, *Elastoplastic Properties of Aluminum Alloy AMg6 with High Strain Rates*, Journal of Applied Mechanics and Technical Physics, **5**, 755–758, 1988.
6. M. WAGENHOFER, M. ERICKSON–NATISHAN, and R. W. ARMSTRONG, *Influences of strain rate and grain size on yield and serrated flow in commercial Al-Mg alloy 5086*, Scripta Materialia, **41**, 1177–1184, 1999.
7. A. H. CLAUSEN, T. BØRVIK, O. S. HOPPERSTAD, and A. BENALLAL, *Flow and fracture characteristics of aluminium alloy AA5083-H116 as function of strain rate, temperature and triaxiality*, Materials Science and Engineering A, **364**, 260–272, 2003.
8. M. J. HADIANFARD, R. SMERD, S. WINKLER, and M. WORSWICK, *Effects of strain rate on mechanical properties and failure mechanism of structural Al-Mg alloys*, Materials Science and Engineering A, **492**, 283–292, 2008.
9. Y. CHEN, A. H. CLAUSEN, O. S. HOPPERSTAD, and M. LANGSETH, *Stress-strain behaviour of aluminium alloys at a wide range of strain rates*, International Journal of Solids and Structures, **46**, 3825–3835, 2009.
10. O. S. LEE and M. S. KIM, *Dynamic material property characterization by using Split Hopkinson pressure bar (SHPB) technique*, Nuclear Engineering and Design, **226**, 119–125, 2003.
11. J. E. FIELD, W. G. WALLEY, W. G. PROUD, H. T. GOLDREIN, and C. R. SIVIOUR, *Review of experimental techniques for high rate of deformation and shock studies*, International Journal of Impact Engineering, **30**, 725–775, 2004.
12. H. KOLSKY, *An Investigation of the Mechanical Properties of Materials at Very High Rates of Loading*, Proceedings of the Physical Society of London, **B62**, 676, 1949.
13. M. A. MEYERS, *Dynamic Behavior of Materials*, New York, John Wiley & Sons, Inc., 1994.
14. M. M. AL–MOUSAWI, S. R. REID, and W. F. DEANS, *The use of the split Hopkinson pressure bar techniques in high strain rate materials testing*, Proceedings of the Institution of Mechanical Engineers, Part C: Journal of Mechanical Engineering Science, **211**, 273–292, 1996.
15. E. D. H. DAVIES and S. C. HUNTER, *The dynamic compression testing of solids by the method of split Hopkinson pressure bar*, Journal of the Mechanics and Physics of Solids, **11**, 155–181, 1963.
16. D. A. GORHAM and X. J. WU, *An empirical method for correcting dispersion in pressure bar measurements of impact stress*, Measurements Science and Technology, **7**, 1227–1232, 1996.
17. ABAQUS/Explicit Manual, *Getting Started with ABAQUS*, Version 6.9.
18. T. BELYTSCHKO, W. K. LIU, and B. MORAN, *Nonlinear Finite Elements for Continua and Structures*, Chichester, John Wiley & Sons, Inc., 2000.

19. G. R. JOHNSON and W. M. COOK, *A Constitutive Model and Data for Metals Subjected to Large Strains and High Temperatures*, [in:] Proceedings of the Seventh International Symposium on Ballistic, Hague, The Netherlands, 1983.
20. T. BØRVIK, A. H. CLAUSEN, M. ERIKSSON, T. BERSTAD, O. S. HOPPERSTAD, and M. LANGSETH, *Experimental and numerical study on the perforation of AA6005-T6 panels*, International Journal of Impact Engineering, **32**, 35–64, 2005.
21. H. RAMÍREZ and C. RUBIO-GONZALEZ, *Finite-Element simulation of wave propagation and dispersion in Hopkinson bar test*, Materials & Design, **27**, 36–44, 2006.

*Received December 23, 2010; revised version June 9, 2011.*

---